Journal of Power Sources 194 (2009) 360–368

Contents lists available at ScienceDirect

Journal of Power Sources

journal homepage: www.elsevier.com/locate/jpowsour

Adaptive supervisory control strategy of a fuel cell/battery-powered city bus

Liangfei Xu, Jianqiu Li*, Jianfeng Hua, Xiangjun Li, Minggao Ouyang

State Key Laboratory of Automotive Safety and Energy, Tsinghua University, Beijing 100084, PR China

ARTICLE INFO

Article history:
Received 22 March 2009
Received in revised form 25 April 2009
Accepted 27 April 2009
Available online 3 May 2009

Keywords:
Fuel cell hybrid vehicle
Fuel economy
Durability
Adaptive supervisory control
Equivalent consumption minimization strategy
Energy management

ABSTRACT

This paper presents an adaptive supervisory control strategy for a fuel cell/battery-powered city bus to fulfill the complex road conditions in Beijing bus routes. An equivalent consumption minimization strategy (ECMS) is firstly proposed to optimize the fuel economy. The adaptive supervisory control strategy is exploited based on this, incorporating an estimating algorithm for the vehicle accessorial power, an algorithm for the battery charge-sustaining and a Recursive Least Squares (RLS) algorithm for fuel cell performance identification. Finally, an adaptive supervisory controller (ASC) considering the fuel consumption minimization, the battery charge-sustaining and the fuel cell durability has been implemented within the hybrid city buses. Results in the "China city bus typical cycle" testing and the demonstrational program of Beijing bus routes are presented, demonstrating that this approach provides an improvement of fuel economy along with robustness and ease of implementation. However, the fuel cell system does not leave much room for the optimal strategy to promote the fuel economy. Benefits may also result in a prolongation of the fuel cell working life, which needs to be verified in future.

1. Introduction

With growing concerns on energy crises and environmental issues, Proton Exchange Membrane (PEM) fuel cell is favored for automotive applications because of zero emission, high efficiency and low noise. However, it has disadvantages of high price and short life-time, which makes the commercialization difficult. The disadvantages could be partly overcome by hybridization [1]. There are two potential benefits by combining a PEM fuel cell with an energy storage source. Firstly, the durability of the fuel cell stack could be improved because the additional energy source can fulfill the transient power demand fluctuations. Secondly, the ability of the energy storage source to recover braking energy enhances the fuel economy greatly [2].

The hybrid configuration raises the question of energy management strategy, to achieve system-level performance objectives such as fuel economy, battery charge-sustaining, fuel cell durability while satisfying the system constraints [3].

The recent literature contains several energy management strategies for Hybrid Electric Vehicles (HEV). Energy management strategies have been investigated for both internal combustion engine hybrid vehicles and fuel cell hybrid vehicles, which shows that there are many common characteristics. These strategies can be categorized into three types: rule-based strategies, instantaneous optimization strategies and global optimization strategies. A rule-based strategy can be easily implemented for the real-time applications based on heuristics. It can be further improved by extracting optimal rules from optimal algorithms [4–6]. An instantaneous optimization strategy evaluates the electrical energy from the battery using an equivalent fuel consumption concept [7–9]. A global optimization strategy minimizes a cost function over a determined driving cycle [10,11]. The global strategy could not be implemented in-vehicle, but it can be regarded as a basis of comparison for the evaluation of other real-time control strategies.

However, still there are some special characteristics for fuel cell hybrid vehicles. The fuel cell voltage drops with increasing current. A reactant starvation occurs at high currents and dynamic loads because the transport of reactant gases is not able to keep pace with the amount used in the reaction. Thus, the fuel cell current and the dynamic of the load need to be limited [12]. Moreover, performance degradation of the PEM fuel cell affects the battery charge-sustaining and the vehicle drivability. An online identification algorithm is therefore necessary to identify the fuel cell performance. Control parameters should be adjusted adaptively in the vehicle supervisory controller to achieve an overall optimal performance.

This paper deals with an adaptive supervisory control strategy of a fuel cell/battery-powered hybrid city bus. It proceeds as follows: Section 2 describes the hybrid powertrain and the city bus. Section 3 details the battery equivalent hydrogen model and the equivalent consumption minimization strategy (ECMS). The adaptive supervisory control strategy based on the ECMS is presented in Section 4, incorporating an estimating algorithm for the

* Corresponding author. Tel.: +86 10 62773437; fax: +86 10 62785708.
E-mail addresses: xuliangfei99@mails.tsinghua.edu.cn (L. Xu), lijianqiu@tsinghua.edu.cn (J. Li).

0378-7753/$ – see front matter © 2009 Elsevier B.V. All rights reserved.
doi:10.1016/j.jpowsour.2009.04.074

Nomenclature

a, b	fit coefficients
b_{fc}	characteristic coefficient of the fuel cell polarization curve (V)
c	fit coefficient
C	hydrogen consumption of the hybrid fuel cell powertrain ($g\,s^{-1}$)
C_{bat}	battery equivalent hydrogen consumption ($g\,s^{-1}$)
C_{fc}	fuel cell hydrogen consumption ($g\,s^{-1}$)
$C_{fc,avg}$	average fuel cell hydrogen consumption ($g\,s^{-1}$)
d, f	fit coefficients
$\boldsymbol{h}$	custom vector
$I_{dc,tg}$	DC/DC target current (A)
I_{fc}	PEM fuel cell net output current (A)
k	coefficient of the energy management strategy (kW)
K	compensation coefficient for battery charge-sustaining
$\boldsymbol{K}$	coefficient matrix
K_1	custom coefficient
$\boldsymbol{P}$	coefficient matrix
P_{bat}	battery power (kW)
$P_{dc,avg}$	average DC/DC output power (kW)
P_{dc0}	fit coefficient (kW)
P_{fc}	fuel cell net power (kW)
R_{chg}	battery charging resistance (Ω)
R_{dis}	battery discharge resistance (Ω)
R_{fc}	characteristic coefficient of the fuel cell polarization curve (Ω)
P_{aux}	vehicle auxiliary power (kW)
$P_{bat,opt}$	battery optimal power (kW)
P_m	electric motor actual output power (kW)
$P_{m,tg}$	electric motor target power (kW)
$P_{mb,tg}$	electric motor target brake power (kW)
$P_{md,tg}$	electric motor target drive power (kW)
Q	battery capacity (A h)
SOC	state of charge
SOC_H	upper limit of SOC
SOC_L	lower limit of SOC
SOC_{tg}	battery target SOC
SOC_1	battery SOC up to the energy management strategy
SOC_2	battery SOC up to the vehicle accessorial power estimatIng algorithm
SOC_3	battery SOC up to the target drive power of the motor $P_{md,tg}$
SOC_4	battery SOC up to the target brake power of the motor $P_{mb,tg}$
$T_{q,tg}$	electric motor target torque (Nm)
V_{bus}	bus voltage (V)
$V_{bus,max}$	maximal bus voltage (V)
$V_{bus,min}$	minimal bus voltage (V)
V_{fc}	fuel cell terminal voltage (V)
V_{fc0}	characteristic coefficient of the fuel cell polarization curve (V)
V_{ocv}	battery open circuit voltage (V)
x_{min}, x_{max}	custom parameters

Greek symbols

$\eta_{chg,avg}$	average charging efficiency
$\eta_{dis,avg}$	average discharging efficiency
η_m	motor efficiency
τ_{dc}	time constant for the low-pass filter (s)
τ_{aux}	time constant for the vehicle accessorial power estimating (s)
μ, κ	custom parameters
ΔSOC	SOC deviation from the target
$\boldsymbol{\theta}$	custom vector
$\hat{\boldsymbol{\theta}}$	estimated value of $\boldsymbol{\theta}$
$\Delta\tau_{dc1}$, $\Delta\tau_{dc2}$, $\Delta\tau_{dc3}$	modified time constants

vehicle accessorial power, an algorithm for the battery charging-sustaining and a Recursive Least Squares (RLS) algorithm for the fuel cell performance identification. Results of the city bus in the "China city bus typical cycle" testing and in the demonstrational program of Beijing are described in Section 5. Section 6 gives the conclusions.

2. The fuel cell hybrid city bus

The approach presented in this paper was implemented in several city buses, which were used as the "pick-up" vehicles in the Marathon Races of the Beijing Olympic and Paralympic Games in 2008. Fig. 1 shows two buses on the Tiananmen Square on 24th August, 2008. Each of them is equipped with ten 140 L/20 MPa hydrogen tanks and weights 14,672 kg.

As electrochemical devices, fuel cells convert chemical energy into electrical energy directly without mechanical processes. PEM fuel cells are especially preferred in automotive applications because they are efficient, compact and have a good ability to follow the dynamic loads. The output power of a single cell with an active area of 200 cm^2 is less than 100 W. Therefore, numerous cells are connected in series to form a multi-kW stack, and a system containing several stacks generates a power output of several tens of kW. Besides, a fuel cell stack also contains several auxiliary subsystems, such as air supply and coolant [2]. For the considered city buses, two stacks with a rated power of 40 kW are electrically connected as parallel strings.

A Ni-MH battery has the advantage of good charging/discharging performance compared to a Pb-acid battery. And it is relatively cheap compared to a Li-ion battery. Thus, a Ni-MH battery with a rated capacity of 80 A h is utilized for the considered city bus. The battery comprises four modules, each of which contains 70 cells. The Ni-MH cells installed in the vehicle have a rated voltage of 1.2 V. Altogether, the 280 cells yield a rated voltage of 338 V. A management system is designed and mounted on the battery to equilibrate the cell voltage, avoid the overcharging of specific cells and measure the working current, the terminal voltage and the temperature.

The city bus is powered by an AC motor with a rated power of 100 kW, a peak power of 150 kW and a maximum torque of 1121 Nm. The fuel cell stack, the Ni-MH battery and the AC motor are con-

Fig. 1. Two PEM fuel cell/battery hybrid city buses on the Tiananmen Square.

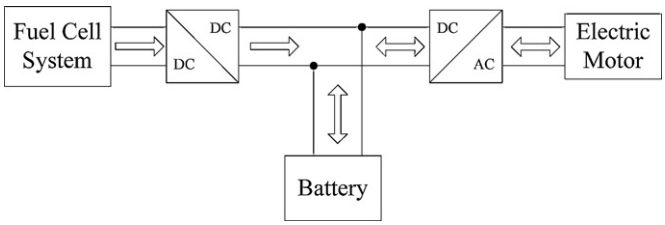

Fig. 2. Structure of the hybrid powertrain and power flow.

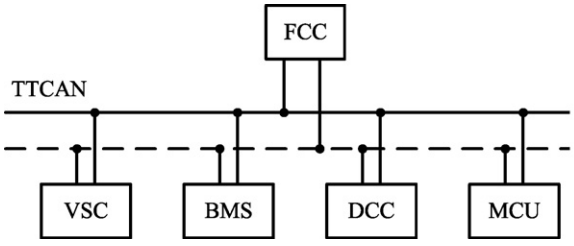

Fig. 3. The time triggered distributed control system based on TTCAN.

nected as shown in Fig. 2. Because the dc bus voltage V_{bus} is lower than the fuel cell terminal voltage V_{fc}, the fuel cell stack is linked to the dc bus by a current-regulated buck converter, which delivers a directional current. A direct current to direct current converter (DC/DC) with a rated power of 80 kW is selected to mach with the PEM fuel cell system.

The hybrid vehicle utilizes the PEM fuel cell as the main power source and the battery as the auxiliary power source. The current-regulated DC/DC is used to control the output power of the fuel cell. The work of the hybrid powertrain is coordinated by a supervisory controller within a TTCAN (Time Triggered Controller Area Network) system, which is shown in Fig. 3.

The TTCAN network communication is based on a periodic time-triggered mechanism. It combines the advantages of event and time triggered communications in distributed real-time control systems. Main advantages of time triggered networks are the quasi deterministic behavior and ease of implementation of fault tolerant systems. One of the disadvantages is the restrictive design process, because the communication structure needs to be defined in advance [12,13].

The time triggered distributed control system comprises a vehicle supervisory controller (VSC), a battery management system (BMS), a DC/DC controller (DCC), a motor controller unit (MCU) and a fuel cell control system (FCC), as shown in Fig. 3. Parameters for the vehicle and the hybrid powertrain are presented in Table 1.

Table 1
Parameters for the vehicle and the hybrid powertrain.

Parameter (unit)	Value
Vehicle mass, m (kg)	1.4672×10^4
Frontal area, A (m^2)	7.5
Drag coefficient, C_D	0.7
Rolling resistance coefficient	1.8×10^{-2}
Mechanical efficiency, η_T (%)	95
Mass factor	1.1
PEM fuel cell rated power (kW)	80
DC/DC rated power (kW)	80
Ni-MH battery rated capacity (A h)	80
Electric motor peak power (kW)	150
Electric motor peak torque (Nm)	1.121×10^3
Electric motor rated power (kW)	100
Electric motor maximal rotational speed ($r\,min^{-1}$)	6×10^3

3. The equivalent consumption minimization strategy (ECMS)

The concept of equivalent fuel consumption was proposed by Paganelli et al. for the development of an instantaneous optimization energy management strategy. In fuel cell hybrid vehicles, both hydrogen energy and electrical energy can be used. If some energy is drawn from the battery at the current sample time, the battery will have to be recharged to maintain the state of charge. The energy will be provided by the fuel cell system. That will imply extra hydrogen consumption. If the battery is recharged at the current sample time, a discharge of the battery is required to maintain the state of charge. This discharge will lead to a reduction of the hydrogen consumption in the future. The electrical energy consumption of the battery is transformed into an equivalent hydrogen consumption to make the two comparable [9,14].

The output power of the fuel cell system is controlled by the current-regulated DC/DC. An optimal DC/DC power $P_{dc,opt}$ is calculated to minimize the hydrogen consumption of the hybrid powertrain C, which comprises the actual fuel consumption C_{fc} and the battery equivalent fuel consumption C_{bat}. Aiming at minimizing the vehicle hydrogen consumption, the equivalent consumption optimization problem is mathematically formulated as follows:

$$P_{dc,opt} = \arg\min_{P_{dc}} C = \arg\min_{P_{dc}} (C_{fc} + \kappa C_{bat}) \tag{1}$$

where P_{dc} is the DC/DC output power (kW). κ is a penalty coefficient, which biases the battery equivalent fuel consumption up or down depending on the battery SOC (state of charge) deviation from the target [3].

The optimization problem is subject to several constrains, such as battery charging-sustaining and respecting the components' limitations:

$$\text{subject to}: \begin{cases} SOC_L \le SOC \le SOC_H \\ V_{bus,min} \le V_{bus} \le V_{bus,max} \\ 0 \le P_{dc} \le P_{dc,max} \end{cases} \tag{2}$$

where SOC_L is the lower limit of SOC, SOC_H is the upper limit of SOC, V_{bus} is the dc-link bus voltage, $V_{bus,max}$ and $V_{bus,min}$ are the maximal and minimal allowed value of V_{bus} and $P_{dc,max}$ is the maximal output power of the DC/DC.

According to the experimental data, the fuel cell hydrogen consumption C_{fc} can be written as:

$$C_{fc} = \begin{cases} aP_{dc} + b & P_{dc} \ge P_{dc0} \\ cP_{dc}^2 + dP_{dc} + f & P_{dc} < P_{dc0} \end{cases} \tag{3}$$

where a, b, c, d, f and P_{dc0} are fit coefficients.

In order to calculate the battery equivalent hydrogen consumption C_{bat}, the average values (average charging/discharging efficiencies, average DC/DC power and average fuel cell hydrogen consumption) are used because the operating points of the PEM fuel cell stack and the battery in the future are not known [9]. This concept is further developed by He et al., where the battery charging/discharging efficiencies are calculated based on the Rint model [15]. Then, the battery equivalent fuel consumption C_{bat} can be written as:

$$C_{bat} = \begin{cases} \dfrac{P_{bat}}{\eta_{chg,avg}} \dfrac{C_{fc,avg}}{P_{dc,avg}} \left(\dfrac{1}{2} + \dfrac{1}{2} \sqrt{1 - \dfrac{4R_{dis}P_{bat}}{V_{ocv}^2}} \right)^{-1} & P_{bat} \ge 0 \\ P_{bat}\eta_{dis,avg} \dfrac{C_{fc,avg}}{P_{dc,avg}} \left(\dfrac{1}{2} + \dfrac{1}{2} \sqrt{1 - \dfrac{4R_{chg}P_{bat}}{V_{ocv}^2}} \right)^{-1} & P_{bat} < 0 \end{cases} \tag{4}$$

A linear penalty coefficient κ is used to accomplish the charge-sustaining operation. It is defined as:

$$\kappa = 1 - 2\mu\frac{(\mathrm{SOC} - 0.5(\mathrm{SOC_H} + \mathrm{SOC_L}))}{\mathrm{SOC_H} - \mathrm{SOC_L}} \tag{5}$$

where μ is a constant, which can be adjusted to reflect the battery charge and discharge characteristics [3].

For the hybrid powertrain under discussion, the fuel cell + DC/DC system works in the linear area during the most of the time on the road. Therefore, the optimized problem defined in Eqs. (1) and (2) could be simplified and the analytic solution to the problem is as follows:

$$\begin{cases} P_{\mathrm{bat,opt}} = \begin{cases} \dfrac{V_{\mathrm{bus,min}}(V_{\mathrm{ocv}} - V_{\mathrm{bus,min}})}{R_{\mathrm{dis}}}, & K_1 \le x_{\mathrm{min}} \\ \dfrac{V_{\mathrm{ocv}}^2(1 - K_1^2)}{4R_{\mathrm{dis}}}, & x_{\mathrm{min}} < K_1 \le 1 \\ 0, 1 < K_1 \le \dfrac{1}{\eta_{\mathrm{chg,avg}}\eta_{\mathrm{dis,avg}}} \\ \dfrac{V_{\mathrm{ocv}}^2(1 - (K_1\eta_{\mathrm{chg,avg}}\eta_{\mathrm{dis,avg}})^2)}{4R_{\mathrm{dis}}}, \dfrac{1}{\eta_{\mathrm{chg,avg}}\eta_{\mathrm{dis,avg}}} < K_1 < \dfrac{x_{\mathrm{max}}}{\eta_{\mathrm{chg,avg}}\eta_{\mathrm{dis,avg}}} \\ -\dfrac{V_{\mathrm{bus,max}}(V_{\mathrm{bus,max}} - V_{\mathrm{ocv}})}{R_{\mathrm{chg}}}, & K_1 \ge \dfrac{x_{\mathrm{max}}}{\eta_{\mathrm{chg,avg}}\eta_{\mathrm{dis,avg}}} \end{cases} \\ P_{\mathrm{dc,opt}} = \max\left(min\left(\dfrac{\pm T_{\mathrm{q,tg}}\omega_{\mathrm{m}}}{\eta_{\mathrm{m}}} + P_{\mathrm{aux}} - P_{\mathrm{bat,opt}}, P_{\mathrm{dc,max}}\right), 0\right) \end{cases} \tag{6}$$

where ω_{m} is the electric motor rotational speed (rad s^{-1}), η_{m} is the electric motor efficiency, P_{aux} is the vehicle auxiliary power (kW), $T_{\mathrm{q,tg}}$ is the electric motor target torque (Nm), $P_{\mathrm{bat,opt}}$ is the battery optimal power (kW), V_{ocv} is the open circuit voltage of the battery (V) and K_1, x_{min}, x_{max} are custom defined variables.

The plus sign "+" is used when the electric motor works as a motor, the minus sign "−" is used when it works as a generator. K_1, x_{min}, x_{max} are defined as:

$$\begin{cases} x_{\mathrm{min}} = \sqrt{1 + 4V_{\mathrm{bus,min}}\left(\dfrac{V_{\mathrm{bus,min}} - V_{\mathrm{ocv}}}{V_{\mathrm{ocv}}^2}\right)} \\ x_{\mathrm{max}} = \sqrt{1 + 4V_{\mathrm{bus,max}}\left(\dfrac{V_{\mathrm{bus,max}} - V_{\mathrm{ocv}}}{V_{\mathrm{ocv}}^2}\right)} \\ K_1 = \dfrac{\kappa}{\eta_{\mathrm{chg,avg}}} \end{cases} \tag{7}$$

$V_{\mathrm{bus,min}}$ and $V_{\mathrm{bus,max}}$ are the minimal and the maximal allowed bus voltages in the hybrid vehicle. V_{ocv} is the open circuit voltage of the battery, which is a function of the battery SOC. Therefore, $P_{\mathrm{bat,opt}}$ is a function of SOC and constant μ.

The constant μ is selected to balance the battery SOC over a whole trip. For the considered bus and the routes in Beijing, 0.6 is a suitable value. Fig. 4 indicates the relationship between $P_{\mathrm{bat,opt}}$ and SOC when μ = 0.6. $\mathrm{SOC_{tg}}$ is the target value of the battery SOC. It is defined as the SOC of the intersection of the battery optimal power curve and the x-axis.

The output current of the DC/DC is regulated to control the output power of the fuel cell stack. A low-pass filter is used to calculate the DC/DC target current $I_{\mathrm{dc,tg}}$ in order to avoid the fuel cell starvation problem under dynamic loads as follows:

$$I_{\mathrm{dc,tg}} = \frac{P_{\mathrm{dc,opt}}/V_{\mathrm{bus}}}{\tau_{\mathrm{dc}}s + 1} \tag{8}$$

where τ_{dc} is the time constant of the low-pass filter and $P_{\mathrm{dc,opt}}$ is calculated as in Eq. (6).

The ECMS referred above is the core of the adaptive supervisory control strategy. However, it is not enough when the bus is driven in bus routes.

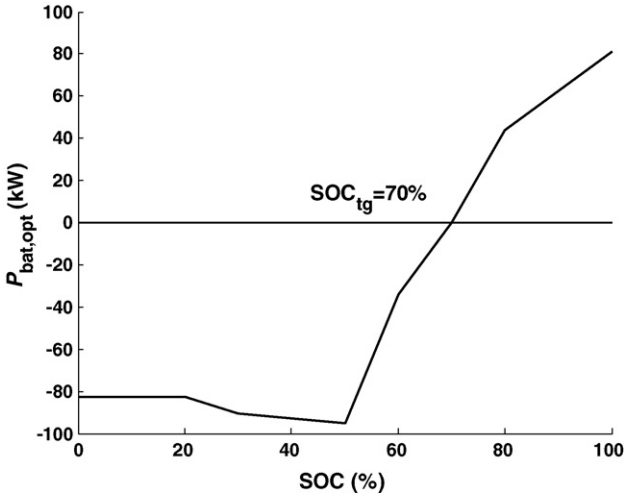

Fig. 4. Relationship between $P_{\mathrm{bat,opt}}$ and SOC when μ = 0.6. $\mathrm{SOC_{tg}}$ is the target value of the battery SOC. It is defined as the SOC of the intersection of the battery optimal power curve and the x-axis.

A lag between the applied load on the fuel cell and the response of the reactant supply system results in an undersupply of reactants to the fuel cell, which leads to a breakdown of the chemical reaction and a rapid loss in voltage [2]. The dynamics of the load need to be restricted to avoid this phenomenon. In the ECMS, the load dynamics are restricted by the low-pass filter with a time constant τ_{dc}. However, the performance of the fuel cell degrades after a long working time. The time constant should be changed according to the status of the fuel cell system. An online identification algorithm for the fuel cell performance is essential.

What is more, the vehicle auxiliary power P_{aux}, which is consumed by the accessorial components, e.g. the air condition and the electric power steering system, changes on the road. The supervisory controller should have the ability to identify the power online. Besides, the battery may be over charged by braking energy when there are too many red lights in the bus route. An algorithm for the battery charge-sustaining is also necessary.

4. The adaptive supervisory control strategy (ASC)

The adaptive supervisory control strategy is developed to fulfill the complex road conditions in bus routes. Based on the ECMS, the adaptive strategy includes three algorithms, an estimating algorithm for the vehicle accessorial power, an algorithm for the battery charge-sustaining and a Recursive Least Square (RLS) algorithm for the fuel cell performance identification.

4.1. The vehicle accessorial power estimating algorithm

The vehicle accessorial power P_{aux} can be calculated as:

$$P_{\mathrm{aux}} = V_{\mathrm{bus}}(I_{\mathrm{dc}} + I_{\mathrm{bat}} - I_{\mathrm{m}}) \tag{9}$$

where I_{dc} is the actual output current of the DC/DC (A). It is measured by the DCC; I_{bat} is the actual output current of the battery (A). It is measured by the BMS; I_{m} is the actual input current of the motor (A). It is measured by the MCU.

However, the result of Eq. (9) includes extra noise, which may be caused by the electromagnetic interference of the electric components in the hybrid powertrain. A low-pass filter is used to extract the actual value. The filtered accessorial power could be expressed as:

$$P_{\mathrm{aux}} = \frac{V_{\mathrm{bus}}(I_{\mathrm{dc}} + I_{\mathrm{bat}} - I_{\mathrm{m}})}{\tau_{\mathrm{aux}}s + 1} \tag{10}$$

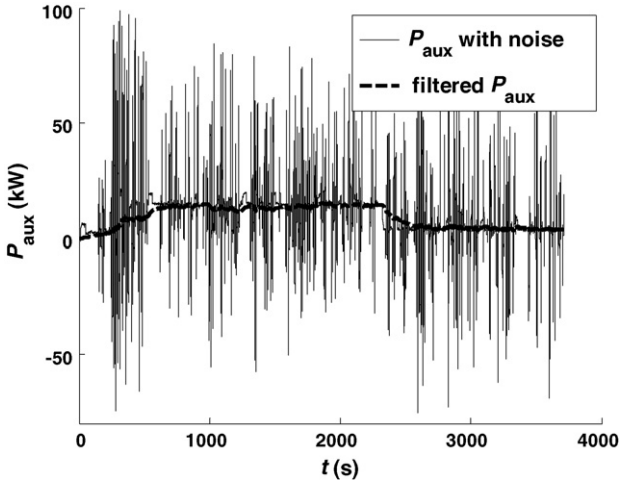

Fig. 5. The original signal of the vehicle accessorial power P_{aux} with extra noise and the filtered P_{aux} with a low-pass filter, τ_{aux} = 100 s.

where τ_{aux} is the time constant. Fig. 5 gives an example of the filtered accessorial power and the original signal with extra noise, τ_{aux} = 100 s.

4.2. The algorithm for the battery charge-sustaining

The battery SOC may deviate from the target on an actual bus route, e.g. a bus route with many red lights. An algorithm is therefore necessary to compensate the SOC deviation from the target.

Based on the ECMS in Section 3 and the estimating algorithm in Section 4.1, the battery SOC could be sketched as in Fig. 6. It can be formulated as:

$$\mathrm{SOC} = \mathrm{SOC}_1 + \mathrm{SOC}_2 + \mathrm{SOC}_3 + \mathrm{SOC}_4 \tag{11}$$

SOC_1 is up to the energy management strategy. It can be written as:

$$\mathrm{SOC}_1 = \frac{k\mathrm{SOC}_{tg}}{V_{ocv}Q\tau_{dc}s^2 + V_{ocv}Qs + k} \tag{12}$$

where Q is the capacity of the Ni-MH battery, k is a coefficient of the ECMS. It is defined as:

$$k = \begin{cases} \dfrac{P_{bat,opt}}{\mathrm{SOC} - \mathrm{SOC}_{tg}}, & \mathrm{SOC} \neq \mathrm{SOC}_{tg} \\ \dfrac{\mathrm{d}P_{bat,opt}}{\mathrm{d}\,\mathrm{SOC}}, & \mathrm{SOC} = \mathrm{SOC}_{tg} \end{cases} \tag{13}$$

SOC_2 is up to the vehicle accessorial power estimating algorithm. It can be expressed as:

$$\mathrm{SOC}_2 = \frac{-P_{aux}(\tau_{dc}\tau_{aux}s^2 + (\tau_{dc} + \tau_{aux})s)}{(V_{ocv}Q\tau_{dc}s^2 + V_{ocv}Qs + k)(\tau_{aux}s + 1)} \tag{14}$$

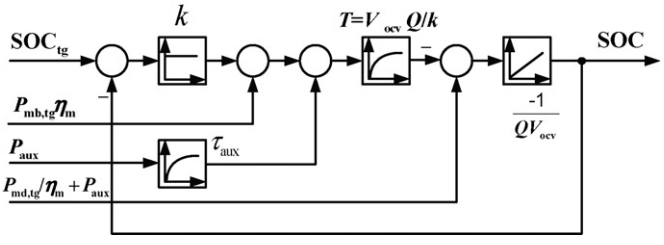

Fig. 6. Sketch diagram of the battery SOC.

SOC_3 depends on the drive power of the motor $P_{md,tg}$. It can be calculated as:

$$\mathrm{SOC}_3 = \frac{-\tau_{dc}/\eta_m s}{V_{ocv}Q\tau_{dc}s^2 + V_{ocv}Qs + k}P_{md,tg} \tag{15}$$

where η_m is the motor efficiency. SOC_4 is up to the brake power of the motor $P_{mb,tg}$. It can be formulated as:

$$\mathrm{SOC}_4 = \frac{-\tau_{dc}\eta_m s - \eta_m}{V_{ocv}Q\tau_{dc}s^2 + V_{ocv}Qs + k}P_{mb,tg} \tag{16}$$

The steady state value of SOC_i, i = 1–4 when $t \to +\infty$ could be calculated as:

$$\begin{cases} \mathrm{SOC}_1|_{t\to\infty} = \dfrac{k\,\mathrm{SOC}_{tg}}{V_{ocv}Q\tau_{dc}s^2 + V_{ocv}Qs + k}|_{s\to 0} = \mathrm{SOC}_{tg} \\ \mathrm{SOC}_2|_{t\to\infty} = 0 \\ \mathrm{SOC}_3|_{t\to\infty} = 0 \\ \mathrm{SOC}_4|_{t\to\infty} = \dfrac{-\eta_m P_{mb,tg}}{k} \end{cases} \tag{17}$$

Thus, the steady deviation of the battery SOC from the target SOC_{tg} is

$$\Delta\mathrm{SOC} = \mathrm{SOC}|_{t\to\infty} - \mathrm{SOC}_{tg} = \frac{-\eta_m P_{mb,tg}}{k} \tag{18}$$

In order to compensate this deviation, the target current of DC/DC should be modified as:

$$I_{dc,tg,modified} = I_{dc,tg} + \frac{Kk\eta_m P_{mb,tg}}{V_{ocv}Qs + k} \tag{19}$$

where K is a compensating coefficient and $I_{dc,tg}$ is calculated as in Eq. (8).

Theoretically speaking, $\Delta\mathrm{SOC} \to 0$ when $t \to +\infty$ if K = 1. To eliminate the deviation in a limited time, K is always larger than 1, depending on the actual bus route. Fig. 7 compares the simulation results of the battery charge-sustaining algorithm with K = 0 (the fine line), K = 1 (the dashed line), K = 2 (the bold line) in a certain bus route.

4.3. The RLS algorithm for the fuel cell performance identification

The output power of the fuel cell system declines after a long driving distance. The performance degradation can be clearly identified by comparing the polarization curves at the beginning and at

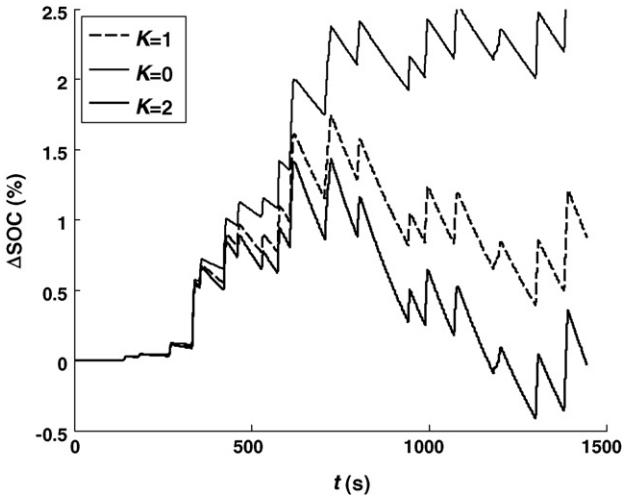

Fig. 7. Comparison of the simulation results of the battery charge-sustaining algorithm with different K, K = 0 (the fine line), K = 1 (the dashed line) and K = 2 (the bold line).

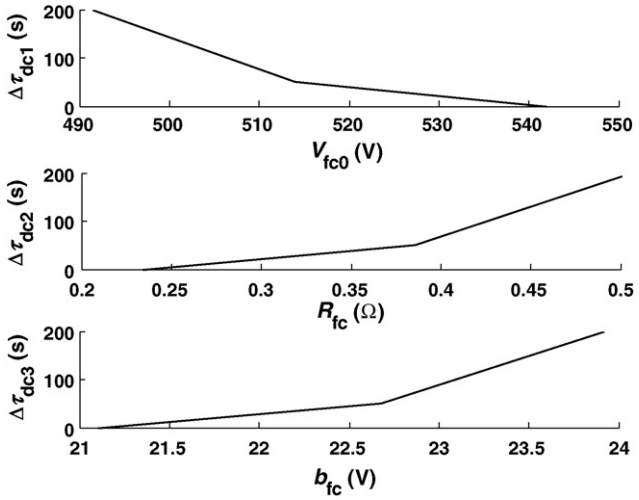

Fig. 8. Relationships between the modified time constants and the parameters for the polarization curve.

the end of a driving distance [16]. The relationship between the fuel cell terminal voltage V_{fc} and its output current I_{fc} can be noted as:

$$\begin{cases} V_{fc} = \boldsymbol{h}^{T}\boldsymbol{\theta} \\ \boldsymbol{\theta} = (V_{fc0}, R_{fc}, b_{fc})^{T} \\ \boldsymbol{h} = (1 - I_{fc} - \ln(I_{fc}))^{T} \end{cases} \quad (20)$$

where $\boldsymbol{h}$ and $\boldsymbol{\theta}$ are vectors, V_{fc0}, R_{fc} and b_{fc} are the characteristic coefficients of the polarization curve [17]. According to the RLS theory, the vector $\boldsymbol{\theta}$ can be estimated as:

$$\begin{cases} \hat{\boldsymbol{\theta}}(k) = \hat{\boldsymbol{\theta}}(k-1) + \boldsymbol{K}(k)[V_{fc}(k) - \boldsymbol{h}(k)^{T}\hat{\boldsymbol{\theta}}(k-1)] \\ \boldsymbol{K}(k) = \boldsymbol{P}(k-1)\boldsymbol{h}(k)[\boldsymbol{h}(k)^{T}\boldsymbol{P}(k-1)\boldsymbol{h}(k) + 1]^{-1} \\ \boldsymbol{P}(k) = [\boldsymbol{I} - \boldsymbol{K}(k)\boldsymbol{h}(k)^{T}]P(k-1) \end{cases} \quad (21)$$

where $\hat{\boldsymbol{\theta}}$ is the estimated value of $\boldsymbol{\theta}$, $\boldsymbol{K}$ and $\boldsymbol{P}$ are coefficient matrixes [18]. The parameters for the fuel cell polarization curve at the beginning of the long driving distance on the testbench are used as the

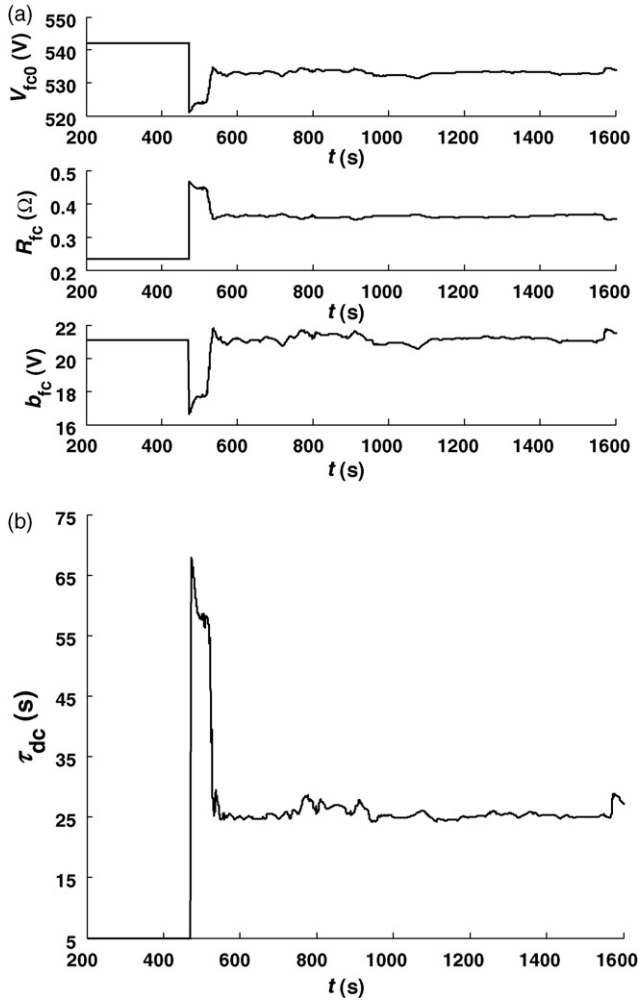

Fig. 9. Simulation results of the RLS algorithm: (a) the three characteristic parameters for the polarization curve and (b) modified time constant $\tau_{dc,modified}$.

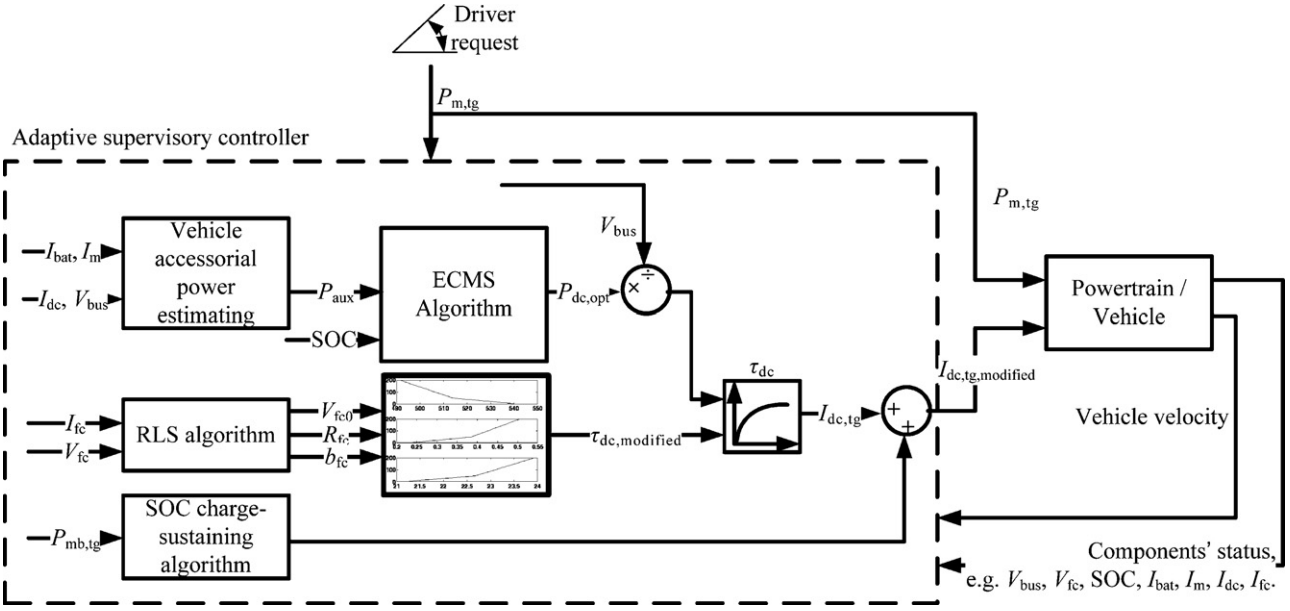

Fig. 10. Implementation of the adaptive supervisory controller (ASC) in the hybrid city bus.

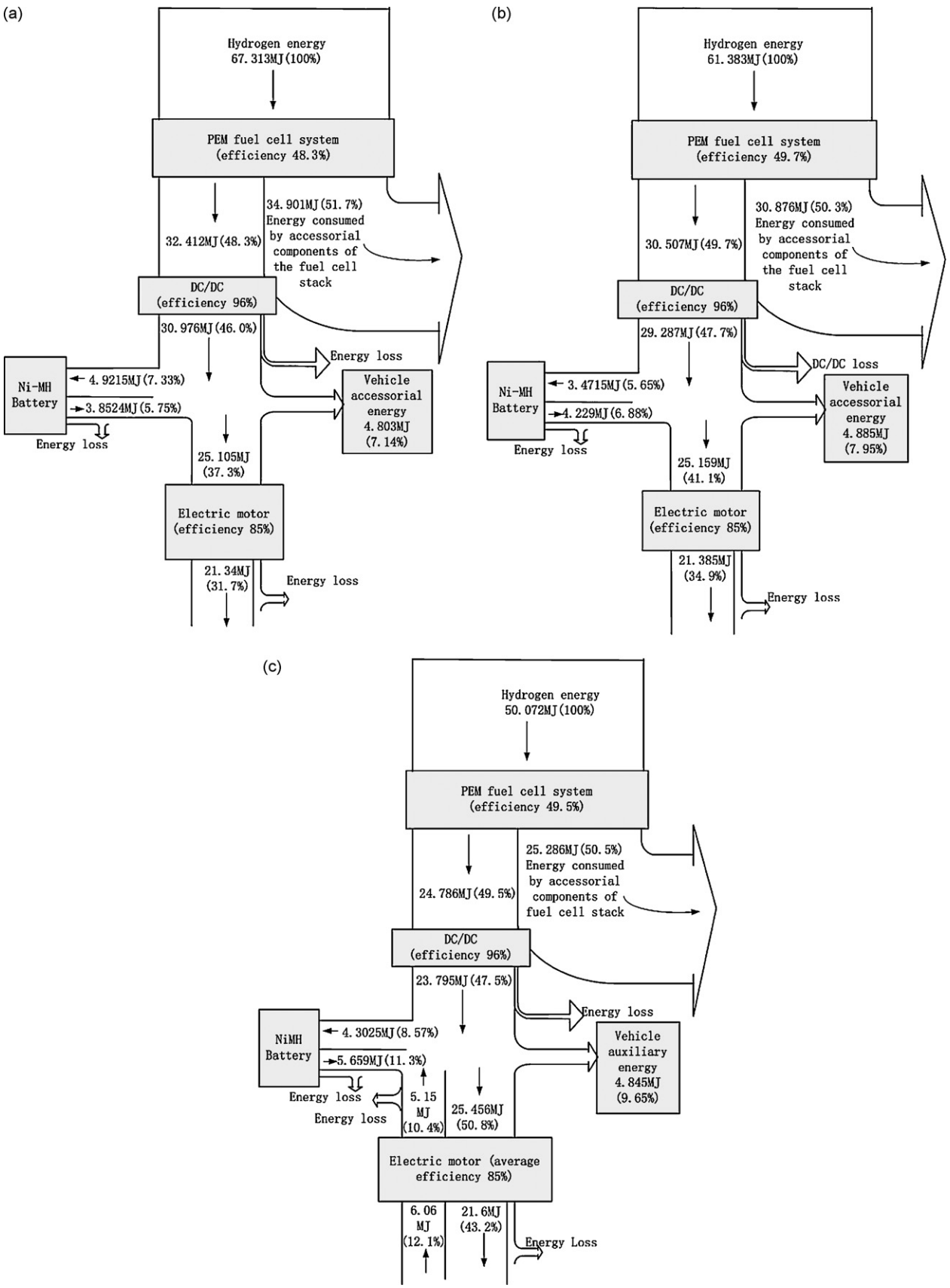

Fig. 11. Energy flow diagrams in the "China city bus typical cycle": (a) a rule-based strategy, (b) the ACS without braking energy regeneration and (c) the ACS with braking energy regeneration.

initial values for the algorithm. They are

$$\hat{\boldsymbol{\theta}}(0) = (\ 542.5059 \quad 0.2337 \quad 21.1059\ )^{\mathrm{T}} \tag{22}$$

The time constant τ_{dc} is then modified according to the results of the RLS algorithm as:

$$\begin{cases} \tau_{dc,modified} = \tau_{dc} + \dfrac{\Delta\tau_{dc1}}{3} + \dfrac{\Delta\tau_{dc2}}{3} + \dfrac{\Delta\tau_{dc3}}{3} \\ \Delta\tau_{dc1} = f_1(V_{fc0}) \\ \Delta\tau_{dc2} = f_2(R_{fc}) \\ \Delta\tau_{dc3} = f_3(b_{fc}) \end{cases} \tag{23}$$

$\Delta\tau_{dc1}$, $\Delta\tau_{dc2}$ and $\Delta\tau_{dc3}$ are the modified time constants, which are functions of V_{fc0}, R_{fc} and b_{fc} respectively. On one hand, performance degradation of the fuel cell stack leads to a decrease in V_{fc0}, an increase in R_{fc} and b_{fc}. On the other hand, a larger DC/DC time constant τ_{dc} is needed to make the output power of the fuel cell stack change much more slowly when the output ability declines. Therefore, $\Delta\tau_{dc1}$ decreases with the V_{fc0} increase, $\Delta\tau_{dc2}$ increases with the R_{fc} increase, $\Delta\tau_{dc3}$ increases with the b_{fc} increase. Fig. 8 gives an example of the three curves.

Fig. 9 gives an example of the RLS algorithm. The estimated parameter converges to a small neighborhood of the actual value a certain period after the system initialization. The parameter is set to the initial value as in Eq. (22) when the estimated result does not converge to the neighborhood. After that, the estimated parameters are used in the energy management strategy. In the given example, the three estimated parameters of the polarization curve are 536 V, 0.38 Ω and 21.2 V respectively. The convergence value appears 600 s after the system initialization. As a result, the DC/DC time constant is adjusted from 5 s to 25 s, which makes the dynamics of the load on the fuel cell much smaller than at the beginning. Thus, the fuel cell stack can work at a quasi-steady state. And the working life of the fuel cell may be prolonged.

5. Results in the cycle testing and the demonstrational program of Beijing bus routes

The implementation of the adaptive supervisory controller (ASC) within the city bus is described in the control scheme shown in Fig. 10. It is a synthetic strategy considering the optimal system efficiency, the battery charge-sustaining and the fuel cell durability. Several city buses with the proposed ASC have been successfully demonstrated in the marathon races of the 29th Olympic and 13th Paralympic Games. Furthermore, they are demonstrated in the Beijing bus routes.

The fuel cell hybrid city buses have been tested in the "China city bus typical cycle" [19,20]. The battery SOC was maintained around 70%. Fig. 11(a)–(c) shows the energy flow diagrams with a rule-based strategy, with the ASC and with the ASC + braking energy regeneration respectively.

The energy flow diagram with a rule-based strategy is shown in Fig. 11(a). The hydrogen chemical energy is calculated on the basis of the LHV (Low Heat Value). Totally 67.313 MJ (100%) was consumed during the cycle testing. Defined as (net power)/(fuel power), the average net efficiency of the fuel cell was about 48.3%, 51.7% of the fuel energy was lost in the stack and its auxiliary components. About 7.14% of the fuel energy was consumed by the vehicle accessorial components. The average efficiencies of the electric motor were 85%. The average powertrain efficiency was about 31.7% and the fuel economy was 9.5 kg (100 km)$^{-1}$.

Fig. 11(b) shows the energy flow diagram with the ASC. Totally 61.383 MJ (100%) was consumed during the cycle. The average net efficiency of the fuel cell was about 49.7%. The average powertrain efficiency was about 34.9% and the fuel economy was 9.3 kg (100 km)$^{-1}$.

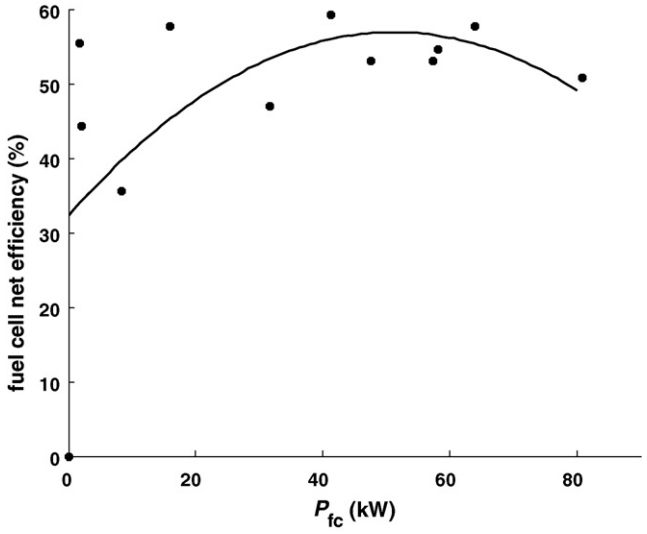

Fig. 12. Fuel cell net efficiency (defined as (net power)/(fuel power)) vs. fuel cell net power. The fitting curve and the experiment data for the considered system.

Fig. 11(c) shows the energy flow diagram with the ASC and the braking energy regeneration. Totally 50.072 MJ (100%) was consumed. The average net efficiency of the fuel cell was about 49.5%. The average powertrain efficiency was about 43.2% and the fuel economy was 7.8 kg (100 km)$^{-1}$.

Compared to the rule-based strategy, the ASC and the braking energy regeneration lower the fuel consumption by 2% and 16% respectively. The braking energy regeneration contributes much more than the ASC to lowering the fuel consumption. This is because the fuel cell system does not leave much room for the optimal strategy to promote the fuel economy. Fig. 12 illustrates the relationship between the fuel cell efficiency and the net power. The fuel cell net efficiency changes slightly between 20 kW and 70 kW. No matter with the ASC or a rule-based strategy, the PEM fuel cell follows the vehicle load demand. Hence, there is not much room left for optimization.

Fig. 13 presents the performance degradation of the fuel cell system during the 8000 km mileage in the demonstrational program. $P_{fc,100A}$ is defined as the net output power of the fuel cell system at a net output current of 100 A. It is regarded as the output ability

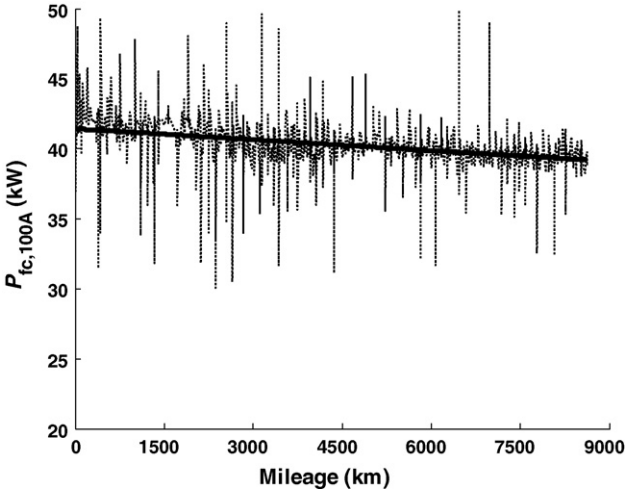

Fig. 13. Performance degradation of the fuel cell system during 8000 km mileage.

of the fuel cell system. The fuel cell performance declines at a rate of $-0.26\,W\,km^{-1}$ ($-0.628\%\,(1000\,km)^{-1}$) according to the on-road data in the 8000 km driving distance. Besides, the battery SOC was always kept around 70% in the bus routes.

6. Conclusions

An adaptive supervisory controller has been exploited considering the fuel economy, the battery charge-sustaining and the fuel cell durability. The control strategy comprises four parts, an ECMS, a vehicle accessorial power estimating algorithm, a battery charge-sustaining algorithm and a RLS algorithm for the fuel cell performance identification.

The analytical solution of the ECMS is derived based on the battery Rint model. The battery optimal power is a function of the battery SOC and a custom defined variable μ, which can be adjusted to reflect the battery charge and discharge characteristics. The SOC deviation is compensated by modifying the DC/DC target current based on the motor braking power and a compensating coefficient K. The variables μ and K should be selected according to the actual bus route.

Compared to a rule-based strategy, the fuel consumption of the city bus with the ASC in the "China city bus typical cycle" was lowered from 9.5 kg $(100\,km)^{-1}$ to 9.3 kg $(100\,km)^{-1}$. It can be lowered to 7.8 kg $(100\,km)^{-1}$ with the ASC + braking energy regeneration strategy. The braking energy regeneration contributes much more than the ASC to lowering the fuel consumption. This is because the fuel cell system does not leave much room for the optimal strategy to promote the fuel economy.

During the 8000 km mileage in the Beijing bus route demonstrational program, the output power of the fuel cell system declines at a rate of $-0.26\,W\,km^{-1}$ ($-0.628\%\,(1000\,km)^{-1}$). The battery SOC was always maintained around 70% in the bus routes.

The proposed approach provides an improvement in fuel economy along with robustness and ease of implementation. Benefits may also result in a prolongation of the fuel cell working life, which needs to be verified in future.

Acknowledgements

Financial support by the Ministry of Science and Technology (MOST) of China and the State Key Lab of Automotive Safety and Energy in Tsinghua University (SKLASE) is gratefully acknowledged.

References

[1] S.J. Kwi, S.O. Byeong, J. Power Sources 105 (2002) 58–65.
[2] P. Rodatz, G. Paganelli, A. Sciarretta, L. Guzzella, Control Eng. Pract. 13 (2005) 41–53.
[3] B. He, M. Ouyang, Int. J. Altern. Propul. 1 (2006) 79–96.
[4] J. Andersson, R. Axelsson, B. Jacobson, JSAE Rev. 20 (1999) 531–536.
[5] S. Aoyagi, Y. Hasegawa, T. Yonekura, H. Abe, JSAE Rev. 22 (2001) 259–264.
[6] N. Jalil, N.A. Kheir, M. Salman, Proc. Am. Control Conf. (1997) 689–693.
[7] Y. Guezennec, T. Choi, G. Paganelli, G. Rizzoni, Proc. Am. Control Conf. 3 (2003) 2055–2061.
[8] K. Oh, D. Kim, T. Kim, C. Kim, H. Kim, KSME Int. J. 18 (2004) 30–36.
[9] G. Paganelli, S. Delprat, T.M. Guerra, J. Rimaux, J.J. Santin, IEEE Veh. Technol. Conf. 4 (2002) 2076–2081.
[10] A. Brahma, Y. Guezennec, G. Rizzoni, Proc. Am. Control Conf. 1 (2000) 60–64.
[11] C.C. Lin, H. Peng, J.W. Grizzle, J. Kang, IEEE Trans. Control Systems Technol. 11 (2003) 839–849.
[12] A. Albert, R. Hugel, Int. CAN Autom. Conf. (2005).
[13] X. Lin, L. Bao, J. Hua, L. Xu, J. Li, M. Ouyang, Fuels and Lubricants Congress, Shanghai, China, 2008-01-1534.
[14] G. Paganelli, M. Tateno, A. Brahma, G. Rizzoni, Y. Guezennec, American Control Conference, Washington, DC, 2001.
[15] V.H. Johnson, J. Power Sources 110 (2002) 321–329.
[16] M. Ouyang, L. Xu, J. Li, L. Lu, D. Gao, Q. Xie, J. Power Sources 163 (2006) 467–479.
[17] S. Srinivasan, O.A. Velev, A. Parthasathy, D.J. Manko, A.J. Appleby, J. Power Sources 36 (1991) 299–320.
[18] Wikipedia, Recursive least squares filter, http://en.wikipedia.org/wiki/Recursive_least_sq-uares_filter.
[19] L. Xu, J. Hua, X. Li, Q. Meng, J. Li, M. Ouyang, IEEE Vehicle Power and Propulsion Conference, Harbin, China, 2008, pp. 1–6.
[20] L. Xu, J. Hua, L. Bao, J. Li, M. Ouyang, SAE Paper 2008-01-1574.